

Learning to predict synchronization of coupled oscillators on heterogeneous graphs

Hardeep Bassi,¹ ^{a)} Richard Yim,² ^{a)} Rohith Kodukula,³ Joshua Vendrow,³ ^{b)} Cherlin Zhu,⁴ and Hanbaek Lyu⁵, ^{c)}

¹⁾Department of Applied Mathematics, University of California, Merced, CA 95343, USA

²⁾Department of Mathematics, University of California, Davis, CA 95616, USA

³⁾Department of Mathematics, University of California, Los Angeles, CA 90095, USA

⁴⁾Department of Applied Mathematics and Statistics, Johns Hopkins University, Baltimore, MD 21218, USA

⁵⁾Department of Mathematics, University of Wisconsin - Madison, WI 53706, USA

Suppose we are given a system of coupled oscillators on an unknown graph along with the trajectory of the system during some short period. Can we predict whether the system will eventually synchronize? Even with known underlying graph structure, this is an important but analytically intractable question in general. In this work, we take a novel approach that we call “learning to predict synchronization” (L2PSync), by viewing it as a classification problem for sets of initial dynamics into two classes: ‘synchronizing’ or ‘non-synchronizing’. While a baseline predictor using concentration principle misses a large proportion of synchronizing examples, standard binary classification algorithms trained on large enough datasets of initial dynamics can successfully predict the unseen future of a system on highly heterogeneous sets of unknown graphs with surprising accuracy. In addition, we find that the full graph information gives only marginal improvements over what we can achieve by only using the initial dynamics. We demonstrate our method on three models of continuous and discrete coupled oscillators — The Kuramoto model, the Firefly Cellular Automata, and the Greenberg-Hastings model. Finally, we show our method applied on larger systems is robust under using initial dynamics partially observed only on some small subgraphs.

I. INTRODUCTION

A. Overview

Many important phenomena that we would like to understand — formation of public opinion, trending topics on social networks, movement of stock markets, development of cancer cells, outbreak of epidemics, and collective computation in distributed systems — are closely related to predicting large-scale behaviors in networks of locally interacting dynamic agents. Perhaps the most widely studied and mathematically intractable of such collective behavior is the *synchronization* of coupled oscillators (e.g., blinking fireflies, circadian pacemakers, BZ chemical oscillators), and has been an important subject of research in mathematics and various areas of science for decades^{1,46}. Moreover, it is closely related to the *clock synchronization* problem, which is essential in establishing shared notions of time in distribution systems, and has enjoyed fruitful applications in many areas including wildfire monitoring, electric power networks, robotic vehicle networks, large-scale information fusion, and wireless sensor networks^{9,39,43}.

For a system of deterministic coupled oscillators (e.g., the Kuramoto model²⁸), the entire forward dynamics (i.e., evo-

lution of phase configurations) is analytically determined by 1) initial phase configuration and 2) graph structure. In this paper, we are concerned with the fundamental problem of *predicting whether a given system of coupled oscillators will eventually synchronize provided with initial dynamics (first few phase configurations) optionally together with graph structure*. More specifically, we consider the following three types of synchronization prediction problem:

Q1 *Given the initial dynamics and graph structure, can we predict whether the system will eventually synchronize?*

Q2 *Given the initial dynamics and not knowing the graph structure, can we predict whether the system will eventually synchronize?*

Q3 *Given the initial dynamics partially observed on a subset of nodes and possibly not knowing the graph structure, can we predict whether the whole system will eventually synchronize?*

An analytical characterization of synchronization would lead to a perfect algorithm for the synchronization prediction problems above. However, while a number of sufficient conditions on model parameters (e.g., large coupling strength) or on initial configuration (e.g., phase concentration into open half-circle) for synchronization are known, obtaining an analytic or asymptotic solution to the prediction question in general appears to be out of reach, especially when the underlying graphs are heterogeneous and the initial phases are not concentrated. In this work, ‘heterogeneous graphs’ refers to sets of non-isomorphic simple graphs, where there is one type of node and edge but the connection topology is diverse. Since

^{a)}Co-first author

^{b)}<http://www.joshvendrow.com>

^{c)}<http://www.hanbaeklyu.com>; Supported by [NSF DMS-2010035](https://www.nsf.gov/awardsearch/showAward?AWD_ID=2010035)

The codes for the main algorithm and simulations are provided in <https://github.com/richpaulyim/L2PSync>

the global behavior of coupled oscillators is built on non-linear local interactions, as the number of nodes increase and the graphs become more heterogeneous, the behavior of the system becomes rapidly intractable. To provide a sense of the complexity of the problem, note that there are more than 10^9 non-isomorphic connected simple graphs with 11 nodes³⁷.

However, the lack of general analytical solution does not necessarily preclude the possibility of successful prediction of synchronization. In this work, we propose a radically different approach to this problem that we call *Learning To Predict Synchronization* (L2PSync), where we view the synchronization prediction problem as a binary classification problem for two classes of ‘synchronizing’ and ‘non-synchronizing’ with features being initial dynamics (optionally with other information). We empirically show that once trained on large enough datasets of synchronizing and non-synchronizing initial dynamics on heterogeneous graphs, a number of standard binary classification algorithms can in fact successfully predict the future of an unknown system with surprising accuracy. We emphasize that these results are achieved without using the graph structure at all, where even simulating the unseen dynamics for prediction is not possible. This may indicate that the entropy of the system would decay rapidly in the initial period to the point that the uncertainty of the future behavior from unknown graph structure becomes not significant. We demonstrate our methods on three models of continuous and discrete coupled oscillators — the Kuramoto model (KM)¹, the Firefly Cellular Automata (FCA)³¹, and the Greenberg-Hastings model (GHM)¹⁹.

The pipeline of our approach is as follows. Namely, 1) fix a model for coupled oscillators; 2) generate a *dynamics dataset* of a large number of non-isomorphic graphs with an even split of synchronizing and non-synchronizing dynamics; 3) train a selected binary classification algorithm on the dynamics dataset to classify each example (initial dynamics with or without underlying graphs) into one of two classes, ‘synchronizing’ or ‘non-synchronizing’; 4) finally, validate the accuracy of the trained algorithms on fresh examples by comparing the predicted behavior of the true long-term dynamics. We use the following classification algorithms: Random Forest (RF)⁴ Gradient Boosting (GB)¹⁶, Feed-forward Neural Networks (FFNN)³, and our own adaptation of Long-term Recurrent Convolutional Networks (LRCN)⁸ which we call the *GraphLRCN*.

As a baseline for our approach, we use a variant of the well-known ‘concentration principle’ in the literature of coupled oscillators. Namely, regardless of the details of graph structure and model, synchronization is guaranteed if the phases of the oscillators are concentrated in a small arc of the phase space *at any given time* (see Subsection IIIA). This principle is applied at each configuration up to the training iteration used to train the binary classifiers. Regardless of the three models of coupled oscillators and selected binary classification algorithm, we find that our method on average shows at least a 30% improvement in prediction performance compared to this concentration-prediction baseline for dynamics on 30 node graphs. In other words, our results indicate that the concentration principle applied at each configuration is too con-

servative in predicting synchronization, and there might be a generalized concentration principle that uses the whole initial dynamics, which our machine learning methods seem to learn implicitly.

For the the question Q3 on synchronization prediction on initial dynamics partially observed on subgraphs, as well as reducing the computational cost of our methods for answering Q1 and Q2, we propose an ‘ensemble prediction’ algorithm (Algorithm 1) that scales up our method to large graphs by training on dynamics observed from multiple random subgraphs. Namely, suppose we are to predict dynamics on connected N -node graphs, where initial dynamics observed on a few small connected subgraphs of $n \ll N$ nodes are available. We first train a binary classification algorithm on the dynamics observed from those subgraphs and then aggregate the predictions from each subgraph (e.g., using majority vote) to get a prediction for the full dynamics on N nodes. Using this method, we achieve an accuracy score of over 85% for predicting the the commonly studied Kuramoto model on 600 node graphs by only using four 30-node subgraphs where the corresponding baseline gets 55% accuracy. In particular, we observe the baseline with locally observed initial dynamics tends to misclassify non-synchronizing examples as synchronizing as locally observed dynamics can concentrate in a short time scale while the global dynamics do not.

From the robustness of our prediction accuracy with respect to both the continuous and discrete models as well as the binary classification algorithm of choice, we believe that our method of ‘learning to predict synchronization’ can be generalized to ‘learning to predict complex systems’.

B. Problem statement and our approach

A graph $G = (V, E)$ consists of sets V of nodes and E of edges. Let Ω denote the *phase space* of each node, which may be taken to be the circle $\mathbb{R}/2\pi\mathbb{Z}$ for continuous-state oscillators or the color wheel $\mathbb{Z}/\kappa\mathbb{Z}$, $\kappa \in \mathbb{N}$ for discrete-state oscillators. We call a map $X : V \rightarrow \Omega$ a *phase configuration*, and say it is *synchronized* if it takes a constant value across nodes (i.e., $X(v) = \text{Const.}$ for all $v \in V$). A *coupling* is a function \mathcal{F} that maps each pair (G, X_0) of graph and initial configuration $X_0 : V \rightarrow \Omega$ deterministically to a *trajectory* $(X_t)_{t \geq 0}$ of phase configurations $X_t : V \rightarrow \Omega$. For instance, \mathcal{F} could be the time evolution rule for the KM, FCA, or GHM. The main problem we investigate in this work is stated below:

Problem I.1 (Synchronization Prediction) *Fix parameters $n \in \mathbb{N}$, $T \gg r > 0$, and coupling \mathcal{F} . Predict the following indicator*

$$\mathbf{1}(X_T \text{ is synchronized}) \quad (1)$$

given the initial trajectory $(X_t)_{0 \leq t \leq r}$ and optionally also with the graph G .

We remark that as T tends to infinity, the indicator (1) converges to the following indicator

$$\mathbf{1}(X_t \text{ is eventually synchronized}), \quad (2)$$

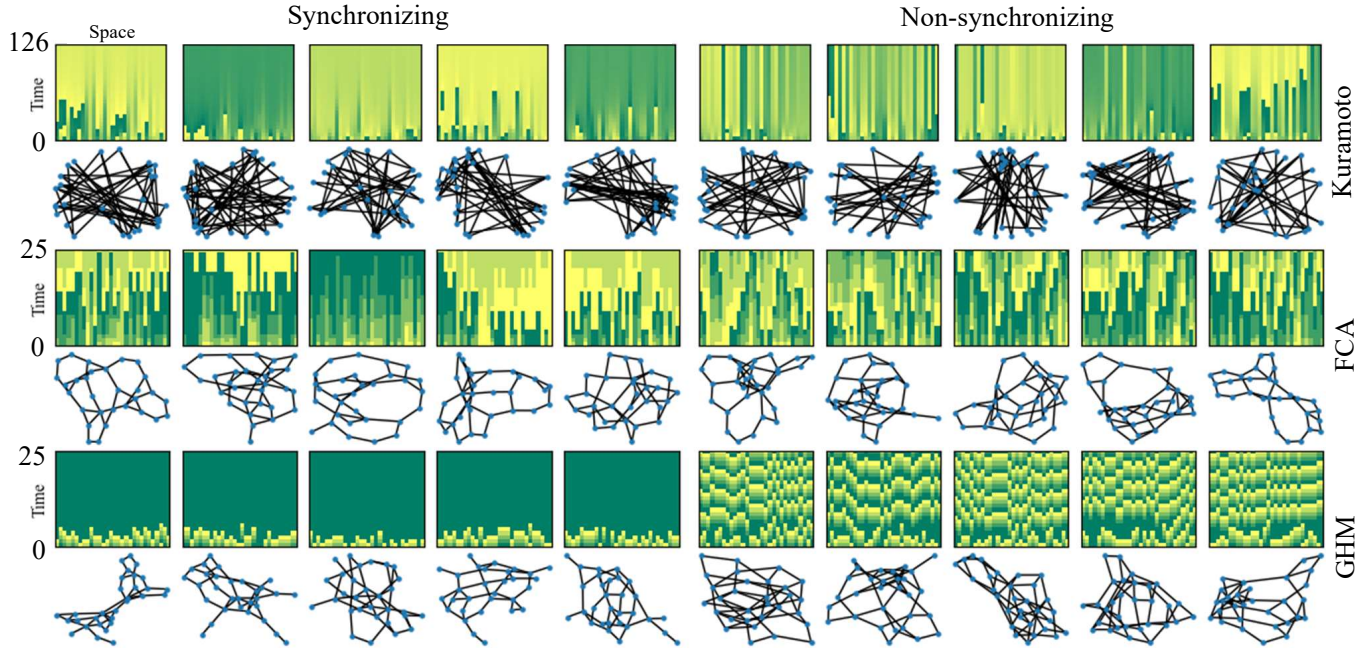


FIG. 1. Sample points in the 30-node dynamics dataset for synchronization prediction. The heat maps show phase dynamics on graphs beneath them, where colors represent phases and time is measured by iterations from bottom-to-top (e.g. $t = 0$ to $t = 25$). Each example is labeled as ‘synchronizing’ if it synchronizes at iteration 1758 for the Kuramoto model (70 for FCA and GHM) and ‘non-synchronizing’ otherwise. Synchronizing examples have mostly uniform color in the top row. For training, only a portion of dynamics is used so that the algorithms rarely see a fully synchronized example (see Figure 4).

which aligns more directly with the initial questions **Q1** and **Q2** than (1). However, determining whether a given system will never synchronize amounts to finding a non-synchronizing periodic orbit, which is computationally infeasible in general. Hence we use (1) as a proxy of (2) in our problem setting. See Figure 4 for an illustration of Problem **L1**.

C. Related works

There are a number of recent works on learning features of dynamical systems from fixed graphs. Itabashi et al.²⁵ used topological data analysis (TDA) to map trajectories of Kuramoto oscillator phases onto a manifold, and extracted time-varying topological features of the dynamics. One of their goals was to learn characterizations of multi-cluster synchronized dynamics at an early stage where oscillators are all-to-all connected, but permitted to form a few clusters. Thiem et al.⁴⁸ used neural networks (NN) to learn coarse-grained dynamics of Kuramoto oscillators and recovered the classical order parameter. Biccari et al.² used gradient descent (GD) and the random batch method (RBM) to learn control parameters to enhance synchronization of Kuramoto oscillators. Slightly less related work is Hefny et al.²⁰, where the authors used hidden Markov models, LASSO regression and spectral algorithms for learning lower-dimensional state representations of dynamical systems, and applied their method on a knowledge tracing model for a dataset of students’ responses to a survey.

References	# nodes	# graphs	# configs.	model	ML
Itabashi et al. ²⁵	128-256	1	100	KM	TDA
Thiem et al. ⁴⁸	1500-8000	1	2000	KM	NN
Biccari et al. ²	10-1000	1	1	KM	GD,RBM
This work	15-600	2K-200K	1	FCA, FFNN, GHM	RF, GB, LRCN

TABLE I. Comparison of settings in related works on learning coupled oscillator dynamics using machine learning methods. Recent works^{2,25,48} focus on learning features of dynamics on fixed graphs. In contrast, we aim to learn how an underlying graph structure influences long-term dynamics. The column for ‘# configs.’ refers to the number of distinct initial phase configurations considered for each graph in training.

It is important to note that the focus of the aforementioned works is to learn features of dynamics on a fixed graph. For this purpose, it is natural to fix an underlying graph (mostly all-to-all) and simulate trajectories from multiple initial configurations and learn features of the generated dynamics. In contrast, our goal is to learn how the underlying structure of a graph influences long-term dynamics. Hence, in our setting we generate a large number (2K-200K) of non-isomorphic graphs (15-600 nodes) with a single initial configuration, and train a machine learning algorithm so that it can correctly classify whether a given graph paired with an initial configuration will eventually synchronize. Random Forest (RF)⁴, Gradient Boosting (GB)¹⁶, Feed-forward Neural Networks (FFNN)³

and Long-term Recurrent Convolutional Networks (LRCN)⁸ are the machine learning models that were applied in our problem. Also, while the works^{2,25,48} only consider the Kuramoto model (KM) and algorithms are trained on graphs with fixed size, we additionally consider two discrete models: Firefly Cellular Automata (FCA)³¹ and the Greenberg-Hastings Model (GHM)¹⁹ and also develop an algorithm where the size of the graph need not be fixed.

We remark that there are a number of cases where rigorous results are available for the question of predicting the long term behavior of a coupled oscillators on a graph G and initial configuration X_0 . For instance, the $\kappa = 3$ instances of GHM and another related model called Cyclic Cellular Automata (CCA)¹² have been completely solved¹⁸. Namely, given the pair (G, X_0) , the trajectory X_t synchronizes eventually if and only if the discrete vector field on the edges of G induced from X_0 is conservative (see¹⁸ for details). Additionally, the behavior of FCA on finite trees is also well-known: given a finite tree T and $\kappa \in \{3, 4, 5, 6\}$, every κ -color initial configuration on T synchronizes eventually under κ -color FCA if and only if κ is strictly less than the maximum degree of T ; for $\kappa \geq 7$, this phenomenon does not always hold^{31,32}. Furthermore, there is a number of works on the clustering behavior of these models on the infinite one-dimensional lattice, \mathbb{Z} (FCA^{34,35}, CCA^{13–15,34} and GHM^{10,34}).

II. BACKGROUNDS

A. Three models for coupled oscillators

The *Kuramoto model* (KM) is one of the most well-studied models for coupled oscillators with continuous states^{1,28,29,46}. Namely, fix a graph $G = (V, E)$ and the continuous state space $\Omega = \mathbb{R}/2\pi\mathbb{Z}$. A given initial phase configuration $X_0 : V \rightarrow \Omega$ evolves via the following systems of ordinary differential equations

$$\frac{d}{dt}X_t(v) = \omega_v + \sum_{u \in N(v)} K \sin(X_t(u) - X_t(v)), \quad (3)$$

for all nodes $v \in V$, where $N(v)$ denotes the set of neighbors of v in G , K denotes the *coupling strength*, and ω_v denotes the *intrinsic frequency* of v . Since we are interested in the dichotomy between synchronization and non-synchronization, we will be assuming identical intrinsic frequencies, which can be assumed to be zero without loss of generality by using a rotating frame. Note that synchronization is an *absorbing state* under this assumption, that is, X_t is synchronized for all $t \geq s$ if X_s is synchronized. In order to simulate KM, we use the following discretization

$$X_{t+h}(v) - X_t(v) = h \left(\sum_{u \in N(v)} K \sin(X_t(u) - X_t(v)) \right), \quad (4)$$

with step size $h = 0.05$. Accordingly, an ‘iteration’ for KM is a single application of the difference equation (4). After a

change of time scale, we write X_k for the configuration obtained after k iterations.

We also consider two discrete models for coupled oscillators. Let $\Omega = \mathbb{N}/\kappa\mathbb{Z}$ be the κ -state color wheel for some integer $\kappa \geq 3$. The κ -color *Firefly Cellular Automata* (FCA) is a discrete-state discrete-time model for inhibitory Pulse Coupled Oscillators (PCOs) introduced by Lyu³¹. The intuition is that we view each node as an identical oscillator (firefly) of κ -states, which *blinks* whenever it returns to a designated *blinking color* $b(\kappa) = \lfloor \frac{\kappa-1}{2} \rfloor$; nodes with post-blinking color $c \in (b(\kappa), \kappa-1]$ in contact with at least one blinking neighbor do not advance, as if their phase update is being inhibited by the blinking neighbors, and otherwise advance to the next color (see Figure 2). More precisely, the coupling for FCA is defined as the following difference equation

$$X_{t+1}(v) - X_t(v) = \begin{cases} 0 & \text{if } X_t(v) > b(\kappa) \text{ and } X_t(u) = b(\kappa) \text{ for some } u \in N(v) \\ 1 & \text{otherwise.} \end{cases} \quad (5)$$

For visualization purposes, it is convenient to consider the equivalent dynamics of ‘centered colorings’ $\bar{X}_t := X_t - t \pmod{\kappa}$, so that if X_t synchronizes, then \bar{X}_t converges to a constant function. In fact, FCA dynamics are displayed in this way in Figures 1 and 4.

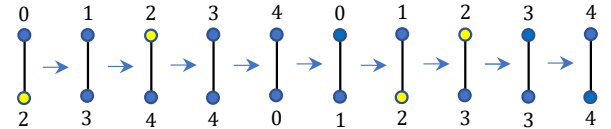


FIG. 2. An example of 5-color FCA dynamics on two connected nodes. $b(5) = 2$ is the blinking color shown in yellow.

On the other hand, the *Greenberg-Hastings model* (GHM) is a discrete model for neural networks¹⁹ introduced in 1987 by Greenberg and Hastings, where nodes of color 0 and 1 are called ‘rested’ and ‘excited’, respectively, and of any other color called ‘refractory’. As in biological neural networks, rested neurons gets excited by neighboring excited nodes, and once excited, it has to spend some time in rested states to come back to the rested state again. More precisely, the coupling for GHM is defined as

$$X_{t+1}(v) = \begin{cases} 0 & \text{if } X_t(v) = 0 \text{ and } X_t(u) \neq 1 \text{ for all } u \in N(v) \\ 1 & \text{if } X_t(v) = 0 \text{ and } X_t(u) = 1 \text{ for some } u \in N(v) \\ X_t(v) + 1 & \text{otherwise.} \end{cases} \quad (6)$$

For GHM, note that X_s is synchronized if and only if $X_t \equiv 0$ for all $t \geq s + \kappa$.

In all experiments in this paper, we consider $\kappa = 5$ instances of FCA and GHM. From here and hereafter, by FCA and GHM we mean the 5-color FCA and 5-color GHM, respectively.

While all three models tend to synchronize locally their global behavior on the same graph and initial configuration

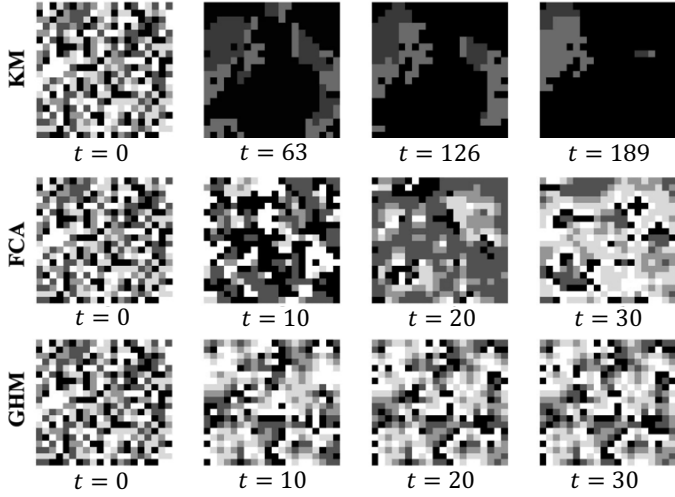


FIG. 3. Simulation of KM, FCA, and GHM on the same underlying graph and initial configuration. The graph is generated by adding 80 edges uniformly at random into 20×20 square lattice. Each square heap map represents a phase configuration X_t at the corresponding iteration t shown below.

evolve quite differently, as seen in Figure 3. There, we simulate each system on the same graph, a 20×20 lattice with an additional 80 edges added uniformly at random. A single initial phase concentration X_0 is chosen by assigning each node with a uniformly randomly chosen state from $\{0, 1, 2, 3, 4\}$. This initial configuration is evolved through three different models: FCA, GHM and KM.

This suggests that it is not feasible to predict synchronization for all three dynamics in the same way. Furthermore, the inclusion of random edges to the square lattice may disrupt some well-known behavior (e.g., spiral waves for coupled oscillators in 2D lattice³⁶) and result in unpredictable dynamics, analytically so. Hence, predicting synchronization on fully heterogeneous sets of graphs (see Figures 1 and 4) is a difficult task since keeping track of local interactions of oscillators is challenging to do when the overall structures of graphs within the heterogeneous set correspondingly have highly irregular and diverse couplings.

III. METHODS

A. The concentration principle for synchronization and baseline predictor

In the literature of coupled oscillators, there is a fundamental observation that concentration (e.g., into an open half-circle) of initial phase of the oscillators leads to synchronization for a wide variety of models on arbitrary connected graphs (see, e.g.,³³ (Lem 5.5)). This is stated in Lemma III.1 for KM and FCA and we call it as the “concentration principle”. This principle has been used pervasively in the literature of clock synchronization^{26,41,42,45} and also in multi-agent consensus problems^{5,38,44}.

Lemma III.1 (Concentration principle) *Let G be an arbitrary connected graph. For Kuramoto model (3) with identical intrinsic frequency and for FCA (5), given dynamics on G synchronizes if all phases at any given time are confined in an open half-circle in the phase space Ω .*

In the above lemma, the ‘open half-circle’ refers to any arc of length $< \pi$ for the continuous state space $\Omega = \mathbb{R}/2\pi\mathbb{Z}$ and any interval of $< \kappa/2$ consecutive integers (mod κ) for the discrete state space $\Omega = \mathbb{Z}/\kappa\mathbb{Z}$. This is a standard fact known to the literature and it follows from the fact that the couplings in the statement monotonically contract given any initial phase configuration under the half-circle condition toward synchronization. An important corollary is the following:

Corollary III.2 *Let G be an arbitrary connected graph. For Kuramoto model (3) with identical intrinsic frequency and for FCA (5), if all states used in the time- t configuration X_t are confined in an open half-circle, then the trajectory on G eventually synchronizes.*

It is not hard to see that Corollary III.2 does not hold for GHM. We define

$$X_t \text{ is concentrated} \quad (7)$$

$$\overset{\text{def}}{\iff} \begin{cases} X_t \text{ is confined in an} \\ \text{open half-circle of } \Omega \end{cases} \quad \begin{array}{l} \text{for KM and FCA} \\ \text{for GHM.} \end{array}$$

We now introduce the following baseline synchronization predictor: Given $(X_t)_{0 \leq t \leq r}$ and $T > r$,

Baseline predictor Predict synchronization of X_T if X_r is concentrated; Otherwise, flip a fair coin.

Notice that by Corollary III.2, the baseline predictor never predicts synchronization incorrectly if X_r is concentrated. For non-concentrated cases, the baseline does not assume any knowledge and gives a completely uninformed prediction. Quantitatively, suppose we use this baseline predictor for a dataset where α proportion of samples are synchronizing where we use the first r iterations of dynamics for each sample. Let $x = x(r)$ denote the proportion of synchronizing samples among all synchronizing samples that concentrate by iteration r . Then the baseline predictor’s accuracy is given by $0.5 + x\alpha/2$, where the second term can be regarded as the gain obtained by using Corollary III.2 layered onto the uninformed decision.

B. Generating the dynamics datasets

We generate a total of nine datasets described in Tables III and IV for studying the synchronization prediction problem (Problem I.1). Data points in each dataset consist of three statistics computed for a pair (G, X_0) of an underlying graph, $G = (V, E)$, and initial configuration, $X_0 : V \rightarrow \Omega$: 1) first r iterations of dynamics $(X_t)_{0 \leq t \leq r}$ (using either KM, FCA, or GHM), (optional) 2) features of G and X_0 , and 3) the label that

indicates whether X_T is concentrated or not (see Table II). We say a data point is ‘synchronizing’ if the label is 1, and ‘non-synchronizing’ otherwise. Every dataset we generate contains an equal number of synchronizing and non-synchronizing examples, and the underlying graphs are all connected and non-isomorphic.

To generate a single n -node graph, we use an instance of the Newman-Watts-Strogatz (NWS) model⁴⁰, which has three parameters n (number of nodes), p (shortcut edge probability), and k (initial degree of nodes)⁷, and an additional integer parameter M (number of calls for adding shortcut edges). Namely, we start from a cycle of n nodes, where each node is connected to its k nearest neighbors. Then we attempt to add a new edge between each initial non-edge (u, v) with probability $p/(n - k - 3)$ independently M times. The number of new edges added in this process follows the binomial distribution with $\binom{n}{2} - \frac{nk}{2}$ trials with success probability $(1 - (1 - \frac{p}{n-k-1}))^M \approx pm/(n - k - 1)$. This easily yields that the expected number of edges in our random graph model is $\frac{nk}{2} + \frac{n^2 p M}{2(n-k-1)} + O(k)$.

The NWS model of random graphs is known to exhibit the ‘small world property’, which is to have a relatively small mean path lengths in contrast to having low local clustering coefficient. This is a widely observed property of many real world complex networks⁴⁰ — as opposed to the commonly studied Erdős-Réyni graphs. It is known that for many models of coupled oscillators are hard to synchronize random initial configuration when the underlying graph is a ring, as discrepancy between oscillators tend to form traveling waves circulating on the ring³⁰. On the other hand, it is observed that coupled oscillator systems on dense graphs are relatively easier to synchronize. Since we intend to generate both synchronizing and non-synchronizing examples to form a balanced dataset, it is natural for us to use a random graph model that sits somewhere between rings and dense graphs. In this sense, NWS is a natural choice of random graph model for our purpose. Using other models such as Erdős-Réyni, for example, generating the balanced dataset of synchronizing and non-synchronizing examples as in Tables III and IV becomes computationally very demanding.

In Table III, we make note of the average graph edge counts and standard deviations of the random graphs that were used to simulate our models on. These characteristics, average edge count and standard deviation of edges counts, correspond to the clustering of edges in the graph, which intuitively affects the propagation of information or states in our cellular automata.

Dynamics	Features	Label
$(X_t)_{0 \leq t \leq r}$	See caption	$\mathbf{1}(X_T \text{ is concentrated}^*)$

TABLE II. Structure of each data point in the dynamics data set. We use the following six features: *number of edges*, *min degree*, *max degree*, *diameter*, *number of nodes*, and *quartiles of initial phases in X_0* . See (7) for the definition of phase-concentration.

In Table III, we give a summary of the six datasets on the three models for two node counts $n = 15, 30$, each with 200K

Datasets	KM ₁₅	KM ₃₀	FCA ₁₅	FCA ₃₀	GHM ₁₅	GHM ₃₀
# nodes	15	30	15	30	15	30
avg of # edges	29.65	57.49	23.91	47.45	22.88	48.18
std of # edges	3.42	5.67	2.34	4.15	2.35	4.11
avg diameter	4.32	7.00	4.32	6.01	4.30	6.12
std of diameter	0.68	1.29	0.67	0.95	0.66	0.98
r (training iter)	126	126	25	25	25	25
T (prediction iter)	1758	1758	70	70	70	70
# Sync.	100K	40K	100K	40K	100K	40K
# Nonsync.	100K	40K	100K	40K	100K	40K

TABLE III. Dynamics datasets generated for three models with two node counts. In each dataset, all graphs are connected and non-isomorphic. # Sync. denotes the number of examples in the dataset such that the phase configuration X_T at iteration T is concentrated (see (7)).

Datasets	FCA ₆₀₀	FCA' ₆₀₀	FCA'' ₆₀₀	KM ₆₀₀	KM' ₆₀₀	KM'' ₆₀₀
# nodes	600	600	300-600	600	600	300-600
std of # nodes	0	0	86.60	0	0	86.60
avg of # edges	2985.53	4749.24	2799.49	1051.08	1109.85	757.89
std of # edges	37.85	2371.72	1461.08	19.66	79.47	56.81
r	50	50	50	400	400	400
T	600	600	600	1758	1758	1758
# Sync.	1K	1K	1K	1K	1K	1K
# Nonsync.	1K	1K	1K	1K	1K	1K

TABLE IV. Dynamics datasets generated for FCA and Kuramoto on 600 nodes (FCA₆₀₀, KM₆₀₀, FCA'₆₀₀, KM'₆₀₀) and on 300-600 nodes (FCA''₆₀₀, KM''₆₀₀). In each dataset, all graphs are connected and non-isomorphic. # Sync. denotes the number of examples in the dataset such that the phase configuration X_T at iteration T is concentrated (see (7)). Here r and T refers to the training and the prediction iterations defined in Table III.

and 80K examples, respectively, which we refer to as KM _{n} , FCA _{n} , GHM _{n} for $n = 15, 30$. Underlying graphs are sampled from the NWS model with parameters $n \in \{15, 30\}$, $M = 1$, and $p = 0.85$ for KM and $p = 0.65$ for FCA and GHM. In all cases, we generated about 400K examples and subsampled 200K and 80K examples for $n = 15, 30$, respectively, so that there are an equal number of synchronizing and non-synchronizing examples, with all underlying graphs as non-isomorphic. The limits for both sets were chosen by memory constraints imposed by the algorithms used. To give a glance of the datasets, we provide visual representations. In Figure 4, we show five synchronizing and non-synchronizing examples in KM₃₀, FCA₃₀, and GHM₃₀ (see (7)).

We also generated six dynamics datasets with a larger number of nodes on FCA and Kuramoto dynamics, as described in Table IV.

The fixed node datasets FCA₆₀₀, FCA'₆₀₀, KM₆₀₀, and KM'₆₀₀ each consist of 1K synchronizing and non-synchronizing examples of FCA and Kuramoto dynamics on non-isomorphic graphs of 600 nodes. The underlying graphs for the fixed node FCA datasets are generated by the NWS model with parameters $n = 600$, $p = 0.6$ and $N = 5$ for FCA₆₀₀ and $p \sim \text{Normal}(\mu_X, 0.04)$, $\mu_X \sim \text{Uniform}(0.32, 0.62)$, for each $N \sim \text{Uniform}(\{1, 2, \dots, 20\})$ calls for FCA'₆₀₀. Similarly, to generate the fixed node Kuramoto datasets, KM₆₀₀ and KM'₆₀₀,

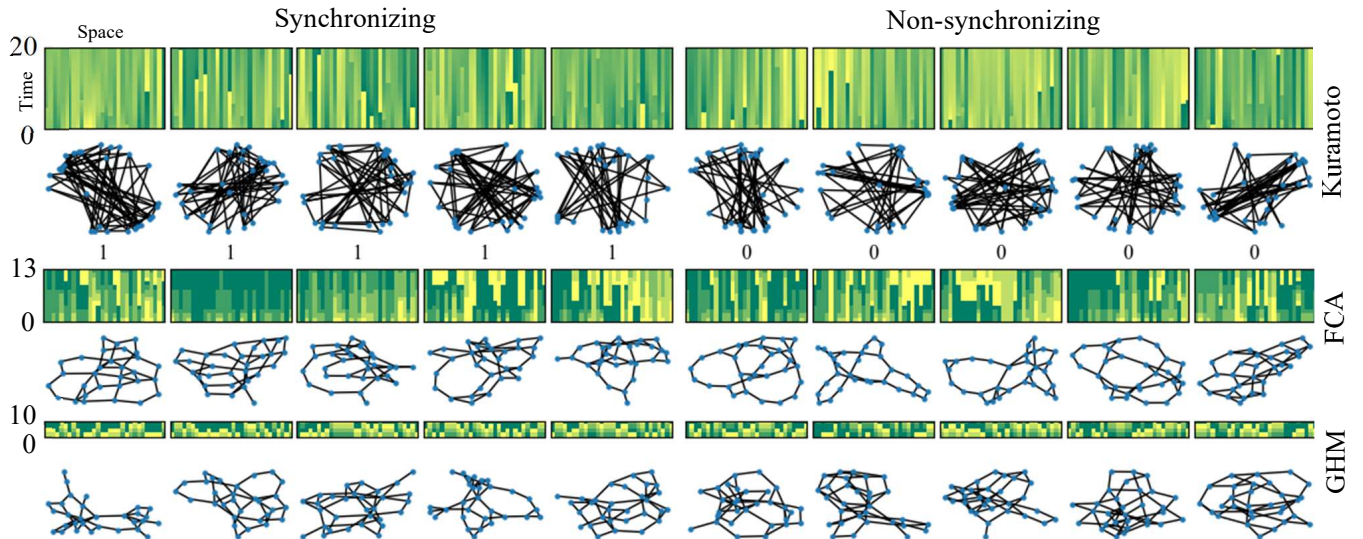


FIG. 4. Sample points in the 30-node training data set for synchronization prediction. The full dataset consists of 40K synchronizing and 40K non-synchronizing 30-node connected non-isomorphic graphs and dynamics on them for each of the three models KM, FCA, and GHM (Table III). With or without the features listed in the caption of Table IV, dynamics up to the first r iterations are used for training. For instance, when $r = 50, 13$, and 4 for KM, FCA, and GHM, respectively, our method using random forest classifier achieves prediction accuracy of 79% (baseline 66%), 84% (baseline 52%), and 89% (baseline 50%) for KM, FCA, and GHM, respectively, trained only with dynamics. See Figure 6. See the caption of Figure 1 for description of the heat maps.

we used the NWS model with parameters $n = 600$, $p = 0.15$ and $N = 5$ for KM_{600} and $p \sim \text{Normal}(\mu_X, 0.04)$, $\mu_X \sim \text{Uniform}(0.32, 0.62)$, for each $N \sim \text{Uniform}(\{1, 2, \dots, 20\})$ calls for KM'_{600} . Consequently, the number of edges in the graphs from KM_{600} and FCA_{600} are sharply concentrated around its mean whereas KM'_{600} and FCA'_{600} have much greater overall variance in the number of edges (see Table IV). For the varied node datasets, FCA''_{600} and KM''_{600} , we kept p distributed in the same way as done for KM'_{600} , FCA'_{600} , but for each $N \sim \text{Uniform}(\{1, 2, \dots, 20\})$ calls of adding shortcut edges, but additionally varied the number of nodes as $n \sim \text{Uniform}(\{300, 301, \dots, 600\})$. In this case, both the number of nodes and edges have relatively greater variation compared to the other datasets.

We omit the Greenberg-Hastings model from this experiment because the dynamics are extremely prone to non-synchronization as a network has more cycles¹¹. Hence, for these large graphs, almost all dynamics following this model will be non-synchronizing. In 40K large networks generated following similar parameters to the FCA_{600} datasets, we found that there was zero synchronizing graphs and 40K non-synchronizing. Hence, there is no real classification problem to be discussed since the presence of synchronizing graphs that follow this model are extremely sparse.

The first two datasets FCA_{600} and FCA'_{600} each consists of 32K synchronizing and non-synchronizing examples of FCA dynamics on non-isomorphic graphs of 600 nodes. The underlying graphs are generated by the NWS model with parameters $n = 600$, $p = 0.6$ and $N = 5$ for FCA_{600} ; and $p \sim \text{Uniform}(0,1)$ for each $N \sim \text{Uniform}(\{1, 2, \dots, 20\})$ calls on FCA'_{600} . Consequently, the number of edges in the graphs from

FCA_{600} are sharply concentrated around its mean whereas FCA'_{600} has much greater overall variance in the number of edges (see Table IV). For the last dataset, FCA''_{600} , we kept $p \sim \text{Uniform}(0,1)$ for each $N \sim \text{Uniform}(\{1, 2, \dots, 20\})$ calls of adding shortcut edges, but additionally varied the number of nodes as $n \sim \text{Uniform}(\{300, 301, \dots, 600\})$. In this case, both the number of nodes and edges have relatively greater variation compared to FCA_{600} .

C. Machine learning algorithms for binary classification

Different machine learning algorithms were employed to solve the problem of predicting whether or not a given graph and initial coloring for a system of coupled oscillators will tend to a synchronizing or non-synchronizing trajectory.

Random Forest (RF)⁴ A random forest is a form of ensemble learning that produces decision trees, and in which these trees themselves are generated using random feature vectors that are sampled independently from a distribution.

Our implementation imposes a limit on the maximum amount of features used per tree to be the square root of the total amount of features in our dataset, \sqrt{p} (where p is the number of features), and uses 100 estimator trees with iterates terminating at complete node purity.

Gradient Boosting (GB)¹⁶ Gradient boosting (GB) is an ensemble learning algorithm for classification tasks similar to RFs where a loss function is minimized by a collection of decision trees to form a strong learner from a group of weak learners. The main difference is that the trees are not trained simultaneously, as in RFs, but added iteratively, so that the

current loss is reduced cumulatively so in each iteration for each tree.

Our implementation uses a learning rate of 0.4, 100 estimator trees, and the square root of total number of features per tree when searching for splits.

Feed-forward Neural Networks (FFNN)³

Neural Networks (FFNN) form a class of function approximators consisting of multiple layers of connected linear and non-linear activation functions^{6,24}. The linear maps are parameterized by ‘weights’, which are subject to training on a given dataset. The algorithm works by iterating two phases. The first phase is the ‘feed-forward’ phase; the input is mapped to an output by applying the layers of linear and non-linear activation functions with the current weights. The loss between the output and the target labels are then computed. The second phase is the ‘back-propagation’ phase; the weights are modified in the direction that reduces the computed loss from the forward propagation phase.

Our implementation of an FFNN uses a learning rate of 0.01, cross-entropy loss, 4 fully connected linear layers, a hidden layer size of 100, ReLU activation, batch normalization, batch size 256, and dropout of 0.25 probability across 35 epochs. See⁴⁷ for backgrounds and jargons.

GraphLRCN A Long-term Recurrent Convolutional Network (LRCN)⁸ is a neural network architecture that has been developed for video data classification by combining convolutional neural networks²⁷ and a special type of recurrent neural network known as the Long Short-Term Memory network (LSTM-Net)²³. We propose a variant of LRCN that is suitable for learning to predict dynamics on graphs, which we call the *GraphLRCN*. The idea is to encode each configuration X_t on a graph G as a weighted adjacency matrix $\Delta(X_t)$ of G . Then the dynamics $(X_t)_{0 \leq t \leq r}$ can be turned into a sequence of square matrices, which can be viewed as video data subject to classification. See Figure 5 for an illustration of GraphLRCN.

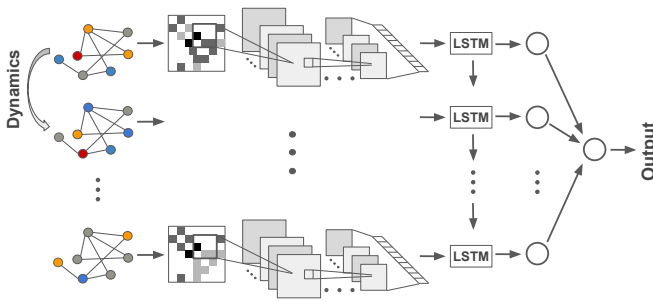


FIG. 5. Architecture of Graph Long-term Recurrent Convolutional Network (LRCN) for synchronization prediction. Dynamics $(X_t)_{0 \leq t \leq r}$ on a graph G are encoded as a sequence of color difference matrices $(\Delta(X_t))_{0 \leq t \leq r}$ and gets fed into the LRCN layers.

Here we give a precise definition of the encoding $X_t \mapsto \Delta(X_t)$. Given a κ -coloring X on a graph $G = (V, E)$, we define the associated *color displacement matrix* $\Delta = \Delta(X)$ as

$(\mathbb{Z}_\kappa)^{|V| \times |V|}$ as

$$\Delta(i, j) = \min \left(\begin{array}{l} X(i) - X(j) \pmod{\kappa}, \\ X(j) - X(i) \pmod{\kappa} \end{array} \right) \mathbf{1}((i, j) \in E). \quad (8)$$

If $X : V \rightarrow [0, 2\pi]$ is a configuration for KM, we define the associated color displacement matrix $\Delta(X)$ similarly as above by replacing $\pmod{\kappa}$ with $\pmod{2\pi}$. One can think of $\Delta(X)$ as the adjacency matrix of G weighted by the color differences assigned by X on the edges. An important feature of this encoding is that $\Delta(X)(i, j)$ is nonzero if and only if nodes i, j are adjacent in G and have different colors $X(i) \neq X(j)$. For instance, if X is synchronized then $\Delta(X)$ is the zero matrix. Additionally, since the convolutional block components learn physical location-based associations in the matrix, we applied the reverse Cuthill-McKee algorithm⁷ on the sequences of adjacency matrices to reduce our matrix bandwidths and augment these physical associations in our representations. In combination, the techniques mentioned are intended to reduce the amount of unnecessary information and noise in the encoding for the purpose of learning to predict synchronization.

D. Learning from locally observed dynamics

In this subsection, we discuss a way to extend our method for the dynamics prediction problem simultaneously in two directions; 1) larger graphs and 2) variable number of nodes. The idea is to train our dynamics predictor on subsampled dynamics of large graphs (specified as induced subgraphs and induced dynamics), and to combine the local classifiers to make a global prediction. In the algorithm below, $f(X_T) := \mathbf{1}(X_T \text{ is concentrated})$, and if X_t is a phase configuration on $G = (V, E)$ and $G_i = (V_i, E_i)$ is a subgraph of G , then $X_t|_{G_i}$ denotes the restriction $v \mapsto X_t(v)$ for all $v \in V_i$.

Algorithm 1 Ensemble Prediction of Synchronization

- 1: **Input:** Dynamics dataset on graphs with $\geq N$ nodes; Test point $(G', (X'_t)_{0 \leq t \leq r})$;
 - 2: **Parameters:** $n_0 \leq N$ (size of subgraphs), $k_{\text{train}}, k_{\text{test}}$ (# of subgraphs), θ (prediction threshold)
 - 3: **Subsample Dynamics:**
 - 4: For each data point $(G, (X_t)_{0 \leq t \leq r}, f(X_T))$:
 - 5: Sample n_0 -node connected subgraphs $G_1, \dots, G_{k_{\text{train}}}$ of G ;
 - 6: Form restricted triples $(G_i, (X_t|_{G_i})_{0 \leq t \leq r}, f(X_T))$
 - 7: **Train Dynamics Predictor:**
 - 8: Train a binary classifier on the restricted triples;
 - 9: **Ensemble Prediction:**
 - 10: Sample n_0 -node connected subgraphs $G'_1, \dots, G'_{k_{\text{test}}}$ of G' ;
 - 11: $\hat{f} :=$ mean of predictions of $f(X_T)$ on subdynamics on G'_i 's
 - 12: **Output:** $\mathbf{1}(\hat{f} > \theta)$
-

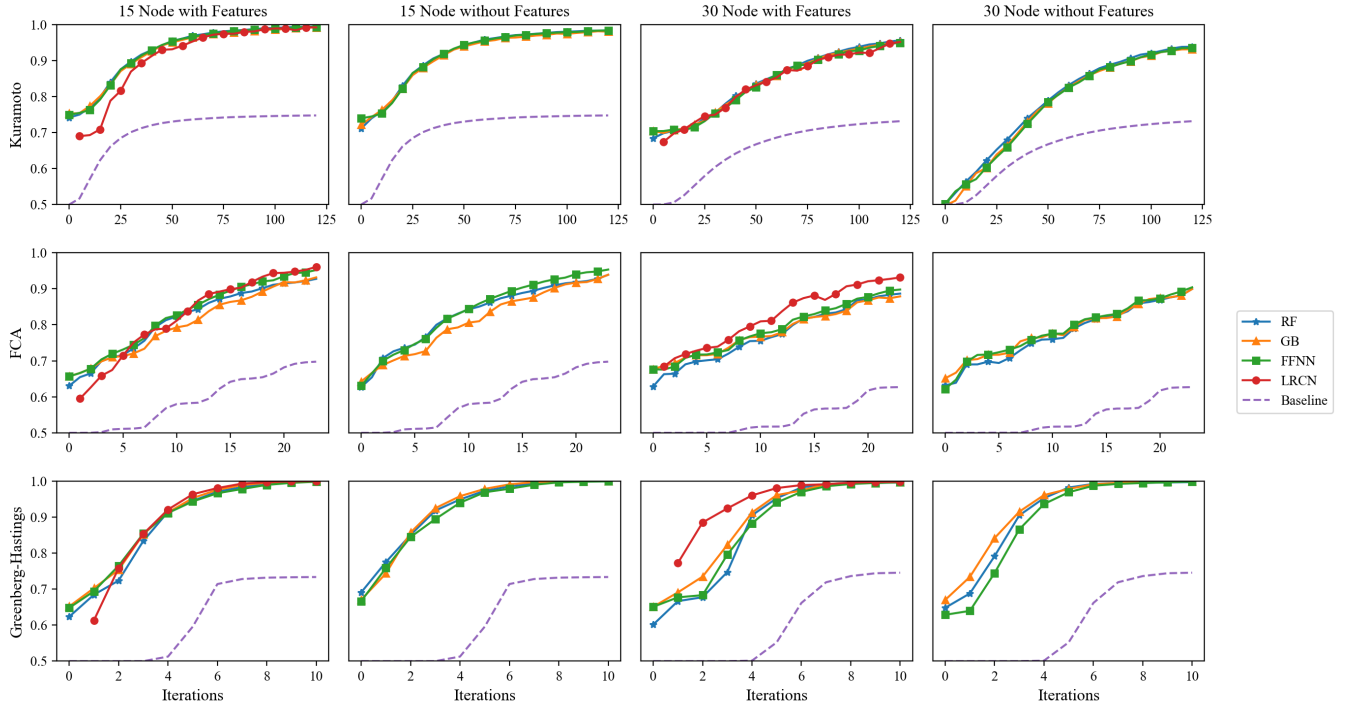


FIG. 6. Synchronization prediction accuracy of four machine learning algorithms for the KM, FCA and GHM coupled oscillators synchronization. For each of the six datasets in Table III, we used 5-fold cross-validation with 80/20 split of test/train. Accuracy is measured by the ratio of the number of correctly classified examples to the total number of examples. Algorithms for the second and the fourth columns are trained only with dynamics up to various iterations indicated on the horizontal axes, whereas the other two columns also use additional feature information in the caption of II.

IV. RESULTS

A. Synchronization prediction accuracy for 15-30 node graphs

We apply the four binary classification algorithms for the six 15-30 node datasets described in Table III in order to learn to predict synchronization. Each experiment uses initial dynamics up to a variable number of training iterations r that is significantly less than the test iteration T , and the goal is to predict whether each example in the dataset is synchronized at an unseen time T (see Problem I.1). We also experiment with and without the additional graph information described in Tables III and II in order to investigate the main questions Q1 and Q2, respectively. We plot prediction accuracy using four classification algorithms (RF, GB, FFNN, LRCN) and the baseline predictor versus the training iteration r , with and without the graph features described in II.

The problem of synchronization prediction becomes easier as we increase the training iteration r . To see this more quantitatively, in Figure 7, we provide the empirical distribution of the first instance (in iterations) to reach phase concentration among all synchronizing examples in datasets KM₃₀, FCA₃₀ and GHM₃₀. Recall that an example with phase concentration will trivially synchronize eventually by Lemma III.1. For instance,

for KM₃₀, there is no trivially synchronizing example at iteration 0, and about 10% of the synchronizing examples will have become phase-concentrated by iteration $r = 25$.

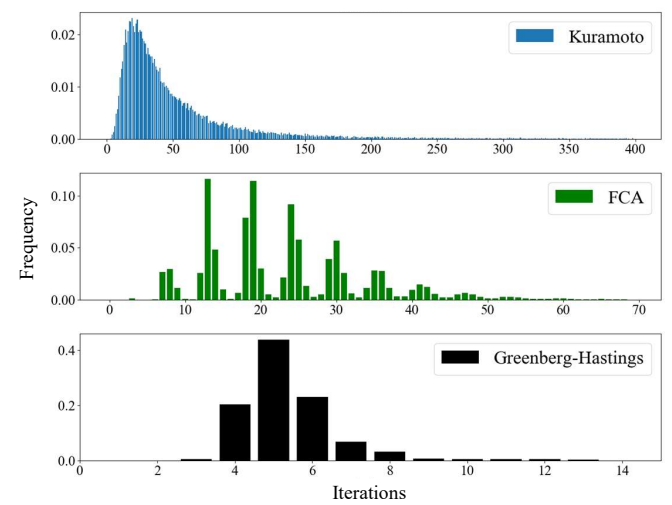


FIG. 7. Empirical distributions on the number of iterations at which synchronizing examples in the dynamics datasets KM₃₀ (top), and FCA₃₀ (middle), GHM₃₀ (bottom) become phase-concentrated.

Now we discuss the results in Figure 6. We see that we are able to achieve results initially ranging from 63% to 74%, by training the FFNN, GB, and RF methods only using the dynamics until training iteration r , and that the long term behavior of each figure at the final training iteration r are all above 90%. This all occurs without the use of the static graph features described in Table II. We see that the KM₃₀ dataset, however, is adversely affected without the use of the graph features and beginning at $r = 0$, we only achieve 50% accuracy initially. This is further discussed in Section IV C along with a systematic analysis on statistical significance of the features to the classification accuracy in more detail. Using the features in Table II along with the dynamics up to iteration r , we see that the classification accuracy at iteration 0 in Figure 6 for the FFNN, GB and RF binary classification methods achieve a classification accuracy ranging from 62% to 75% and all increase to above 90% accuracy. On the other hand, the GraphLRCN binary classifier is offset with respect to the other algorithms as it is fed dynamics information encoded into the adjacency matrix of the underlying graph as in (8), so it cannot be trained only with dynamics information. Often times, GraphLRCN begins below the classical algorithms, but is able to outperform them in intermediate iterations, but by the final training iteration, there is only a negligible difference in the performance over different classifiers.

Second, we find that as we train the binary classifiers on additional dynamics information, the classification accuracy improves for all cases and for all classifiers; additionally, all four classifiers significantly outperform the baselines in all cases. The classifiers show similar performance for KM and FCA, and the GraphLRCN classifier consistently outperforms the other models, especially so with GHM on 30 nodes. For instance, when $r = 20, 10$ and 4 for KM₃₀, FCA₃₀ and GHM₃₀, respectively, our best method (GraphLRCN) achieves a prediction accuracy of 73% (baseline 55%, 1.25% concentrates), 84% (baseline 52%, 1% concentrates) and 96% (baseline 50%, 0% concentrates), respectively. Furthermore, it appears that GHM appears to be the easiest to predict synchronization among the three models we compared above. For instance, for both GHM₁₅ and GHM₃₀, training all four classifiers on only $r = 4$ training iterations without graph features produces a prediction accuracy of at least 90% both with and without the use of graph features, while the baseline achieves only 50%, meaning that no synchronizing example is phase-concentrated by $r = 4$ iterations. This suggests that there is some condition on the phase concentration, *different* from phase-concentration, that most synchronizing examples under the GHM dynamics exhibit by iteration $r = 4$, and that such condition is detected by our machine learning algorithms. A further investigation is due to exactly pin-point what such an alternative evidentiary condition for synchronization is exactly.

Overall, we conclude that the prediction accuracies we are able to achieve using various binary classification methods are virtually unaffected by further including the features of the underlying graph in Table II for training. Also, we observe that if we increase the amount of training iterations over time, each algorithm is able to produce significantly higher accuracy for

distinguishing a synchronizing and non-synchronizing examples against the baseline predictor based on the concentration lemma III.1.

B. Synchronization prediction accuracy for 300-600 node graphs

In this section, we investigate Question Q3, which is to predict synchronization only based on local information observed on select subgraphs. Note that this is difficult task than Q2, since not only we may not have information about the underlying graph but we also may not have observed the entire phase configuration. For example, the dynamics may appear to be synchronized at local scale (e.g., on 30-node connected subgraphs), but there is still large-scale waves being propagated and the global dynamics is not synchronized. Nevertheless, we can use the ensemble prediction method (Algorithm 1) to combine decisions based on each subgraph to predict synchronization of the full graph.

In Figures 8 and 9, we report the synchronization prediction accuracy of the ensemble predictor (Algorithm 1) on datasets FCA₆₀₀, FCA₆₀₀, FCA''₆₀₀, and KM₆₀₀, KM₆₀₀, KM''₆₀₀, respectively, described in Table IV. We used Algorithm 1 with $n_0 = 30$ (size of subgraphs), $k \in \{1, 2, 4, 8\}$ (# of subgraphs). The binary classification algorithm we used is the FFNN. As the baseline, we use a slight modification of the baseline predictor in Section III A. Namely, we combine all phase values observed on all k subgraphs, and predict synchronization if they satisfy the concentration condition (7) and otherwise we flip a fair coin. Note that concentration of phases observed on subgraphs does *not* imply synchronization of the full system, as the full phase configuration may not be concentrated.

So far we have been using the metric of accuracy for our synchronization prediction task, which is defined as the ratio of the correctly predicted synchronizing and non-synchronizing examples to the total number of examples in the dataset. There are multiple ways that this metric could be low, for example if an algorithm is overly conservative and misses lots of synchronizing examples or in the opposite case it may incorrectly classify lots of non-synchronizing examples. In order provide a better insights on these aspects, we also report the performance of our method (Algorithm 1) and the baseline in terms of precision and recall. Here, *precision* is formally defined as the proportion of positive classifications that are correct, or $\frac{TP}{TP+FP}$, where TP is "true positive" and FP is "false positive." In our problem, this corresponds to what proportion of predictions in synchronization were truly correct. *Recall* is formally defined as the proportion of accurately identifying true labels in the data, or $\frac{TP}{TP+FN}$, where FN is "false negative." Again with respect to our prediction problem, measuring recall corresponds to how well a given algorithm, ensemble or baseline, correctly identifies synchronization behavior when presented with synchronizing data.

Our accuracy results for both the ensemble method and baseline are presented in Figures 8 and 9 for Kuramoto and FCA models, respectively. In these figures, the first columns represents the results for the datasets $\{\text{KM}, \text{FCA}\}_{600}$ with fixed number of nodes (600) and relatively smaller variation of edge

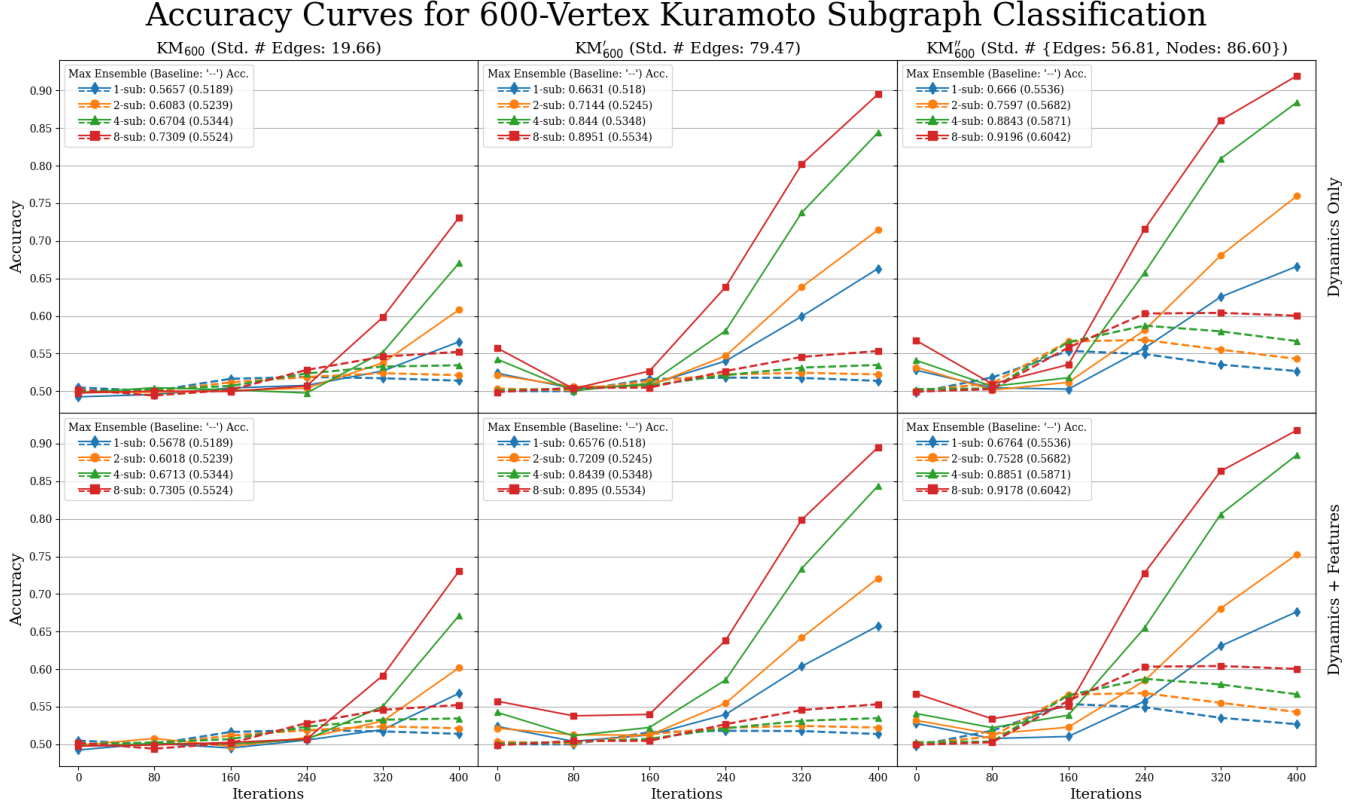


FIG. 8. Accuracy curves for predicting synchronization of Kuramoto on 600-node graphs from dynamics observed from $k \in \{1, 2, 4, 8\}$ subgraphs of 30 nodes. All plots observe the performance of both the ensemble machine learning (solid) and baseline (dashed) accuracies over increasing amounts of training iterations $r \in \{0, 80, 240, 320, 400\}$. The first row shows results using only dynamics whereas the second row includes both the dynamics and graph features. Maximum accuracies for using k subgraphs are given by ‘ k -sub: Acc. (Baseline Acc.)’

counts ($\text{std} \approx 20, 38$, respectively); the second columns for the datasets $\{\text{KM}, \text{FCA}\}'_{600}$ with fixed number of nodes (600) and relatively larger variation of edge counts ($\text{std} \approx 80, 2371$, respectively); and the third for the datasets $\{\text{KM}, \text{FCA}\}''_{600}$ with varied number of nodes ($\text{std} \approx 86$) and relatively larger variation of edge counts ($\text{std} \approx 1461, 56$, respectively). The first rows of both figures represent prediction accuracies using exclusively dynamics data, and the second row utilizing both dynamics and graph features. In the appendix ??, Figures 11 and 12 show the recall and precision curves of the ensemble and baseline methods with the same row and column orientation as the accuracy figures representing different graph datasets and subsets of features. For the Kuramoto data in Figure 8, we applied the ensemble and baseline algorithms cumulatively up to training iterations $r = 0, 80, 160, 240, 320$ and 400; and for the FCA data in Figure 9, we applied the ensemble and baseline algorithms cumulatively up to training iterations $r = 0, 10, 20, 30, 40$ and 50 (Note that using $r = 0$ means fitting the prediction algorithms at the initial coloring). We additionally remark that these curves were averaged over 30 train-test splits with 80% training and 20% testing.

Across all datasets considered, we see that our ensemble method consistently outperforms the baseline method in accuracy at training iterations $r = 400$ for Kuramoto and $r = 50$ for

FCA. For example, across all Kuramoto datasets and feature subsets by the last iteration, $r = 400$, the ensemble method on a single subgraph outperforms the baseline algorithm on eight subgraphs; the best that the baseline algorithm does is 60.42% accuracy compared to the 91.96% for the ensemble method’s best accuracy. For FCA, the baseline accuracy is 70.29% compared to the best ensemble method score of 85.79%, both on eight subgraphs. Considering the recall and the precision plots in Figures 11 and 12 gives more detailed explanation. Namely, the ensemble method significantly outperforms the baseline in recall by at least 35%, whereas it performs relatively worse in precision than the baseline by at most 10% for both Kuramoto and FCA with $k = 8$ subgraphs except for the datasets KM_{600} . This means the baseline is ‘too conservative’ in the sense that it misses correctly classifying a large number of synchronizing examples. From this, we deduce that a large number of synchronizing examples exhibit phase concentration over subgraphs much later in the dynamics—making early detection through phase concentration difficult. On the contrary, the high recall scores of the ensemble methods indicate that our method can still detect most of the synchronizing examples by only using local information observed on the selected subgraphs. To elaborate, the baseline only determines phase concentration at a single point in time, whereas the ensem-

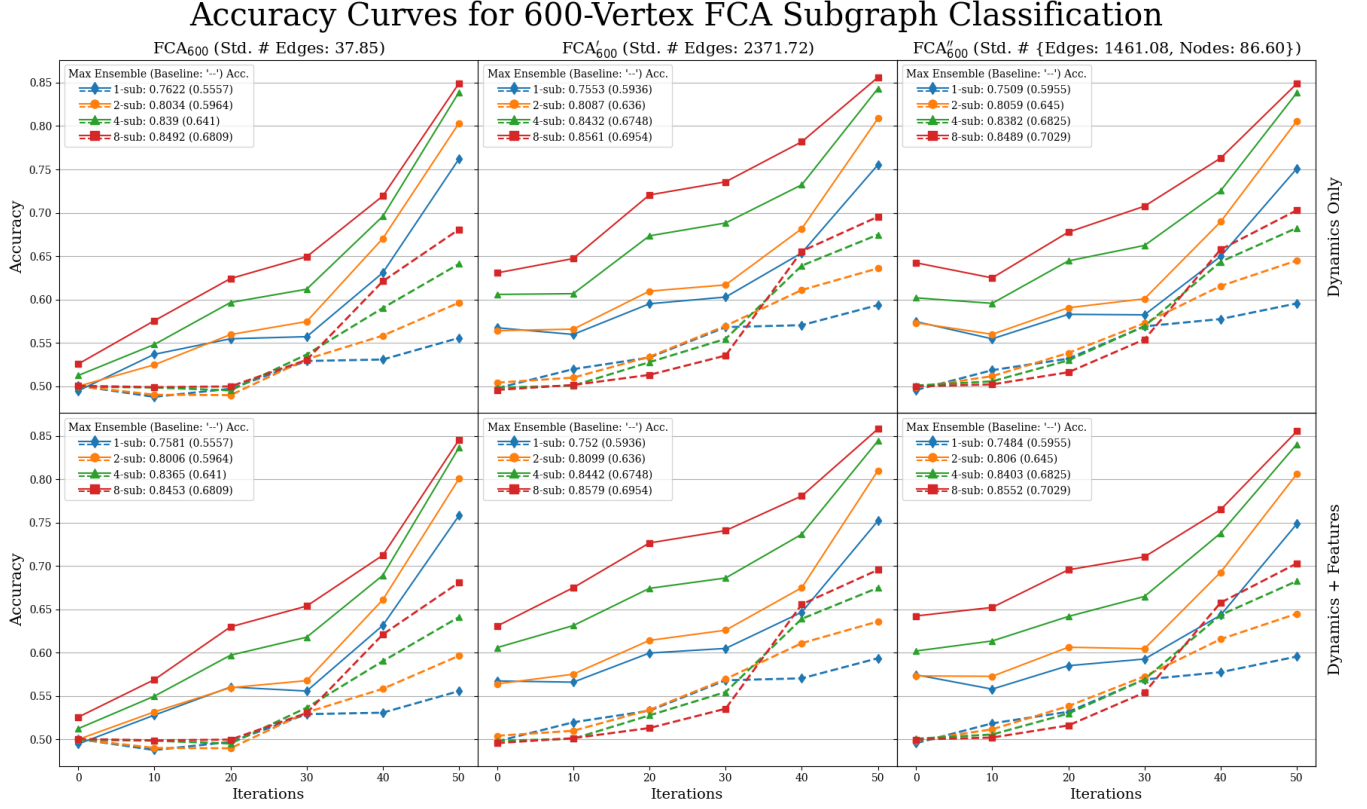


FIG. 9. Accuracy curves for predicting synchronization of 5-color FCA on 600-node graphs from dynamics observed from $k \in \{1, 2, 4, 8\}$ subgraphs of 30 nodes. All plots observe the performance of both the ensemble machine learning (solid) and baseline (dashed) accuracies over increasing amounts of training iterations $r \in \{0, 80, 240, 320, 400\}$. The first row shows results using only dynamics whereas the second row includes both the dynamics and graph features. Maximum accuracies for using k subgraphs are given by ‘ k -sub: Acc. (Baseline Acc.)’

ble method is able to learn the whole variation of dynamics up to iteration r . Furthermore, between training our data on dynamics only, versus dynamics and graph features, across accuracy, recall and precision curves, the inclusion of graph features hardly improves the maximum score of these values.

Finally, for both Kuramoto and FCA, we observe that high variation of the node and edge counts boosts all performance metrics of accuracy, recall, and precision. For example, for recall curves, we see that for varied edge count, compared to fixed edge count, recall is considerably higher than fixed edge count by iteration 400, comparing a recall rate of 0.8755 and 0.9759 for 8 subgraphs, 0.1 point gap. Furthermore, the performance gain in introducing larger variation of node and/or edge counts is significantly larger for Kuramoto than FCA. We speculate that having larger variation of node and edge counts within the dataset presumably implies better separation between the synchronizing and the non-synchronizing examples in the space of initial dynamics. We remark that the performance gain here is not due to a better separation between the classes in terms of the graph features, we can see by comparing the first and the second rows of all figures (Figures 8-12).

C. Discussion

In Figure 6, observe that not using the additional graph features as input (column 4) decreases the prediction accuracy from 70% to 50% for the case of KM_{30} at initial training iteration $r = 0$, but there is no such significant difference for the discrete models FCA_{30} and GHM_{30} . In fact, in all experiments we perform in this work (those reported in Figures 6, 8, 9, 11, and 12), this is only instance that we see that including the graph features during training affects the prediction accuracy.

In order to explain why this is case, we comparing statistical significance of the all features (including the initial coloring, see Table II) we use for the prediction task. We do so by computing the Gini indexes of all features by repeating the prediction experiment over 300 train/test splits of the datasets KM_{30} , FCA_{30} , GHM_{30} using GB for the choice of binary classifier. The analysis using GB will be representative of all other binary classifiers since there is negligible differences in their performance in Figure 6.

As mentioned before, the procedure works by fitting random subsets of features and iteratively growing decision trees; it also records what is known as the Gini index²² over each consecutive partition through multiple training iterations. As decision trees split the feature space, the Gini index mea-

sures total variance across classes—in our case, synchronizing v.s. non-synchronizing —, over each partition. Allowing the supposition that synchronization can be modeled through our graph features data using the gradient boosting method, observing the mean decrease in the Gini index across decision trees allows us to infer feature importance for synchronization over different models and graphs. See, Hartman et al.²² for more discussions on GB and computing the Gini index.

Interestingly, the discrete models models of FCA and GHM place significantly greater importance on color statistics such as the initial quartile colorings, and less importance on graph features such as diameter and minimum and maximum degree. Note that the initial color statistics can be directly computed from the initial dynamics even at training iteration $r = 0$, so this explains that there is no significant performance difference in prediction accuracy for the discrete models in Figure 6. On the contrary, the Kuramoto model puts greater importance on graph features such as diameter and number of edges rather than the initial color statistics, and such graph features are not available from the information given by the initial dynamics at training iteration $r = 0$. From this, we can see why our algorithms show low prediction accuracy in the case of KM₃₀. In addition, we note that there is only a negligible difference in prediction accuracy for KM₁₅ in Figure 6. We speculate that this is because for KM₁₅, as we see in Table III, having only 15 nodes does not allow to have significant variation in the diameter and the edge counts of the graphs in the dataset.

Lastly, we remark that synchronization behavior of Kuramoto model on complete graphs are well-understood in the literature of dynamical systems^{1,28,46}. In our experiments, we observed that graphs with small diameter tend to be synchronizing, and this aligns with the literature since graphs with the same number of nodes but with smaller diameter are closer to complete graphs.

D. Conclusion

Predicting whether a given system of coupled oscillators with an underlying arbitrary graph structure will synchronize is an important yet analytically intractable problem. In this work, we proposed an alternative approach to this problem by viewing it as a binary classification task, where each data point consisting of initial dynamics (optionally with graph information) needs to be classified into two classes of ‘synchronizing’ and ‘non-synchronizing’ dynamics. We have shown that, once trained on large enough datasets of synchronizing and non-synchronizing dynamics on heterogeneous graphs, standard binary classification algorithms can indeed be successfully trained and used to predict the synchronization of unknown systems with accuracy far exceeding a baseline utilizing the well-known “concentration principle” in dynamical systems. These results are achieved without using the graph structure at all, where even simulating the unseen dynamics for prediction is infeasible. Furthermore, we have also shown that our methods are robust under using incomplete initial dynamics only observed on a few small subgraphs.

Drawing conclusions from our machine learning ap-

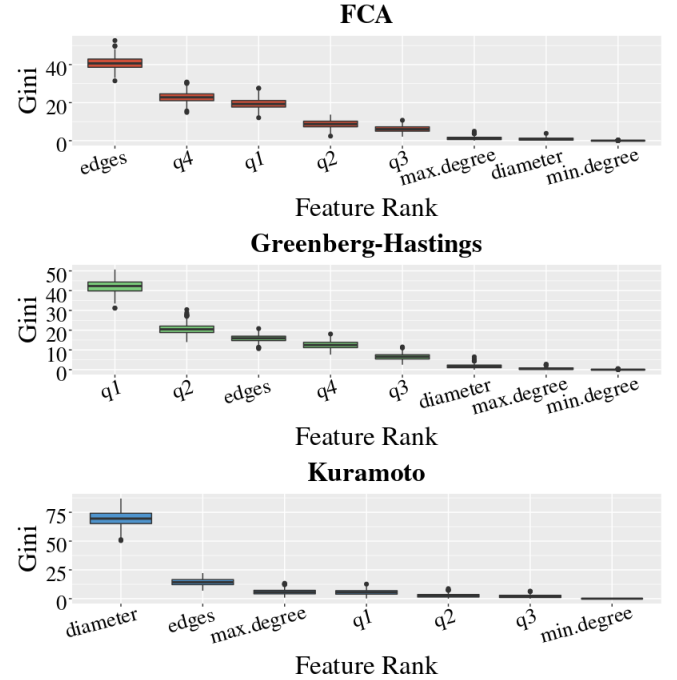


FIG. 10. Boxplots of Gini index values sampled from gradient boosting procedure. Color information appears to be very important according to the distribution of Gini index values in both the FCA and GH models, discrete cellular automata models, and diameter overwhelmingly appears to have the greatest importance for Kuramoto.

proaches to the synchronization prediction problem, we pose the following hypotheses:

- The entropy of the dynamics of coupled oscillators may decay rapidly in the initial period to the point that the uncertainty of the future behavior from unknown graph structure becomes not significant.
- The concentration principle applied at any given time is too conservative in predicting synchronization, and there might be a generalized concentration principle that uses the whole initial dynamics, which our machine learning methods seem to learn implicitly.

Given that our machine learning approach is able to achieve high prediction accuracy, we suspect that there may be some analytically tractable characterizations on graphs paired with corresponding initial dynamics signaling eventual synchronization or not, which we are yet to establish rigorously. As mentioned at the end of Subsection IC, previously known of such characterizing conditions include the initial vector field on the edges induced by the initial color differential for the 3-color GHM and CCA¹⁷, as well as the number of available states being strictly less than the maximum degree of underlying trees for the FCA^{31,32}. Designing similar target features into datasets and training binary classification algorithms could guide further analytic discovery of such conditions for the coupled oscillator models considered in this work.

Furthermore, even though we have focused on predicting only two classes of long-term behavior of complex dynamical systems as only synchronizing and non-synchronizing dynamics, our method can readily be extended to predicting an arbitrary number of classes of long-term behaviors. For instance, one can consider the κ -state voter model on graphs, where the interest would be the final dominating color. In such circumstances, one can train κ -state classification machine learning algorithms on datasets of heterogeneous graphs. Beyond κ -state classification our method can be extended to predicting a continuous variable that is associated to a complex dynamical systems on graphs. For instance, if each node in a graph represents a particular stock in a financial model, could one predict the long-term value of a portfolio given by the ensemble of such stocks that interact with each other? For such problems, one could train a regression model on datasets generated on heterogeneous graphs to gain insights on how the limiting aggregate value of the entire system of interacting assets is influenced by the underlying graph structure.

Finally, a more ambitious task beyond long-term dynamic behavior quantified by a single metric is the potential extension of our methods to full time-series and graph state regression. In other words, if each node in the graph represents an individual in an arbitrary social network, can we predict the sentiment level for a given topic at any given time t for every single individual in that particular social network? One can again generate large overarching social networks and run many simulations of sentiment dynamics with many possible edge configurations between individuals (for example, measured by the number of mutual friends or likes/shares of posts on social media). The ultimate goal would be a framework for learning to predict, with precision, entire trajectories of complex dynamical systems.

ACKNOWLEDGMENTS

This work is supported by NSF grant [DMS-2010035](#). We are also grateful for partial supports from and the Department of Mathematics and the Physical Sciences Division at UCLA. We also thank Andrea Bertozzi and Deanna Needell for supports and helpful discussions. JV is partially supported by Deanna Needell's grant NSF BIGDATA DMS #1740325.

REFERENCES

- ¹Juan A Acebrón, Luis L Bonilla, Conrad J Pérez Vicente, Félix Ritort, and Renato Spigler. The kuramoto model: A simple paradigm for synchronization phenomena. *Reviews of modern physics*, 77(1):137, 2005.
- ²Umberto Biccari and Enrique Zuazua. A stochastic approach to the synchronization of coupled oscillators. 2020.
- ³Christopher M Bishop. *Pattern recognition and machine learning*. Springer, 2006.
- ⁴Leo Breiman. Random forests. *Machine learning*, 45(1):5–32, 2001.
- ⁵Bernard Chazelle. The total s-energy of a multiagent system. *SIAM Journal on Control and Optimization*, 49(4):1680–1706, 2011.
- ⁶Balázs Csanád Csáji et al. Approximation with artificial neural networks. *Faculty of Sciences, Eötvös Loránd University, Hungary*, 24(48):7, 2001.
- ⁷Elizabeth Cuthill and James McKee. Reducing the bandwidth of sparse symmetric matrices. In *Proceedings of the 1969 24th national conference*, pages 157–172, 1969.
- ⁸Jeffrey Donahue, Lisa Anne Hendricks, Sergio Guadarrama, Marcus Rohrbach, Subhashini Venugopalan, Kate Saenko, and Trevor Darrell. Long-term recurrent convolutional networks for visual recognition and description. In *Proceedings of the IEEE conference on computer vision and pattern recognition*, pages 2625–2634, 2015.
- ⁹Florian Dorfler and Francesco Bullo. Synchronization and transient stability in power networks and nonuniform kuramoto oscillators. *SIAM Journal on Control and Optimization*, 50(3):1616–1642, 2012.
- ¹⁰Richard Durrett and Jeffrey E Steif. Some rigorous results for the greenberg-hastings model. *Journal of Theoretical Probability*, 4(4):669–690, 1991.
- ¹¹Richard Durrett and David Griffeath. Asymptotic behavior of excitable cellular automata. *Experimental mathematics* 2.3 183–208, 1993.
- ¹²Robert Fisch. Cyclic cellular automata and related processes. *Physica D: Nonlinear Phenomena*, 45(1):19–25, 1990.
- ¹³Robert Fisch. The one-dimensional cyclic cellular automaton: a system with deterministic dynamics that emulates an interacting particle system with stochastic dynamics. *Journal of Theoretical Probability*, 3(2):311–338, 1990.
- ¹⁴Robert Fisch. Clustering in the one-dimensional three-color cyclic cellular automaton. *The Annals of Probability*, pages 1528–1548, 1992.
- ¹⁵Robert Fisch, Janko Gravner, and David Griffeath. *Cyclic cellular automata in two dimensions*. Springer, 1991.
- ¹⁶Jerome H Friedman. Stochastic gradient boosting. *Computational statistics & data analysis*, 38(4):367–378, 2002.
- ¹⁷Janko Gravner, Hanbaek Lyu, and David Sivakoff. Limiting behavior of 3-color excitable media on arbitrary graphs. *Annals of Applied Probability (to appear)*, 2016.
- ¹⁸Janko Gravner, Hanbaek Lyu, David Sivakoff, et al. Limiting behavior of 3-color excitable media on arbitrary graphs. *The Annals of Applied Probability*, 28(6):3324–3357, 2018.
- ¹⁹James M Greenberg and SP Hastings. Spatial patterns for discrete models of diffusion in excitable media. *SIAM Journal on Applied Mathematics*, 34(3):515–523, 1978.
- ²⁰Ahmed Hefny, Carlton Downey, and Geoffrey Gordon. Supervised learning for dynamical system learning. 2015.
- ²¹Hagberg, Aric and Swart, Pieter and S Chult, Daniel Exploring network structure, dynamics, and function using NetworkX. *Los Alamos National Lab.(LANL), Los Alamos, NM (United States)*, 2008.
- ²²Hartmann, C and Varshney, Pramod and Mehrotra, Kishan and Gerberich, C. Application of information theory to the construction of efficient decision trees. *IEEE Transactions on information theory*, 28(4):565–577, 1982.
- ²³Sepp Hochreiter and Jürgen Schmidhuber. Long short-term memory. *Neural computation*, 9(8):1735–1780, 1997.
- ²⁴Kurt Hornik. Approximation capabilities of multilayer feedforward networks. *Neural networks*, 4(2):251–257, 1991.
- ²⁵Kazuha Itabashi, Quoc Hoan Tran, and Yoshihiko Hasegawa. Evaluating the phase dynamics of coupled oscillators via time-variant topological features. 2020.
- ²⁶Johannes Klinglmayr, Christoph Kirst, Christian Bettstetter, and Marc Timme. Guaranteeing global synchronization in networks with stochastic interactions. *New Journal of Physics*, 14(7):073031, 2012.
- ²⁷Alex Krizhevsky, Ilya Sutskever, and Geoffrey E Hinton. Imagenet classification with deep convolutional neural networks. *Communications of the ACM*, 60(6):84–90, 2017.
- ²⁸Yoshiki Kuramoto. *Chemical oscillations, waves, and turbulence*. Courier Corporation, 2003.
- ²⁹Tony E. Lee, Heywood Tam, G. Refael, Jeffrey L. Rogers, and M. C. Cross. Vortices and the entrainment transition in the two-dimensional kuramoto model. *Physical Review E*, 82(3), Sep 2010.
- ³⁰Sofianti Lee and Raymond Lister. Experiments in the Dynamics of Phase Coupled Oscillators When Applied to Graph Colouring *Proc. 31st Australasian Computer Science Conference (ACSC 2008)*, 2008.
- ³¹Hanbaek Lyu. Synchronization of finite-state pulse-coupled oscillators. *Physica D: Nonlinear Phenomena*, 303:28–38, 2015.
- ³²Hanbaek Lyu. Phase transition in firefly cellular automata on finite trees. *arXiv preprint arXiv:1610.00837*, 2016.

- ³³Hanbaek Lyu. Global synchronization of pulse-coupled oscillators on trees. *To appear in SIAM Journal on Applied Dynamical Systems. Preprint available at arXiv:1604.08381*, 2017.
- ³⁴Hanbaek Lyu and David Sivakoff. Persistence of sums of correlated increments and clustering in cellular automata. *Submitted. Preprint available at arXiv.org/1706.08117*, 2017.
- ³⁵Hanbaek Lyu and David Sivakoff. Synchronization of finite-state pulse-coupled oscillators on \mathbb{Z} . *arXiv.org:1701.00319*, 2017.
- ³⁶Erik A Martens, Carlo R Laing, and Steven H Strogatz. Solvable model of spiral wave chimeras. *Physical review letters*, 104(4):044101, 2010.
- ³⁷Brendan McKay. Combinatorial data. <http://users.cecs.anu.edu.au/~bdm/data/graphs.html>, 2020.
- ³⁸Luc Moreau. Stability of multiagent systems with time-dependent communication links. *Automatic Control, IEEE Transactions on*, 50(2):169–182, 2005.
- ³⁹Sujit Nair and Naomi Ehrich Leonard. Stable synchronization of rigid body networks. *Networks and Heterogeneous Media*, 2(4):597, 2007.
- ⁴⁰Mark EJ Newman, Duncan J Watts, and Steven H Strogatz. Random graph models of social networks. *Proceedings of the National Academy of Sciences*, 99(suppl 1):2566–2572, 2002.
- ⁴¹Joel Nishimura and Eric J Friedman. Robust convergence in pulse-coupled oscillators with delays. *Physical review letters*, 106(19):194101, 2011.
- ⁴²Felipe Nunez, Yongqiang Wang, and Francis J Doyle. Synchronization of pulse-coupled oscillators on (strongly) connected graphs. *Automatic Control, IEEE Transactions on*, 60(6):1710–1715, 2015.
- ⁴³Roberto Pagliari and Anna Scaglione. Scalable network synchronization with pulse-coupled oscillators. *IEEE Transactions on Mobile Computing*, 10(3):392–405, 2011.
- ⁴⁴Antonis Papachristodoulou, Ali Jadbabaie, and Ulrich Munz. Effects of delay in multi-agent consensus and oscillator synchronization. *Automatic Control, IEEE Transactions on*, 55(6):1471–1477, 2010.
- ⁴⁵Anton V Proskurnikov and Ming Cao. Synchronization of pulse-coupled oscillators and clocks under minimal connectivity assumptions. *arXiv preprint arXiv:1510.02338*, 2015.
- ⁴⁶Steven H Strogatz. From kuramoto to crawford: exploring the onset of synchronization in populations of coupled oscillators. *Physica D: Nonlinear Phenomena*, 143(1):1–20, 2000.
- ⁴⁷Daniel Svozil, Vladimir Kvasnicka, and Jiri Pospichal. Introduction to multi-layer feed-forward neural networks. *Chemometrics and intelligent laboratory systems*, 39(1):43–62, 1997.
- ⁴⁸Thomas N. Thiem, Mahdi Kooshkbaghi, Tom Bertalan, Carlo R. Laing, and Ioannis G. Kevrekidis. Emergent spaces for coupled oscillators. *Frontiers in Computational Neuroscience*, 14:36, 2020.

Appendix A: Additional Plots

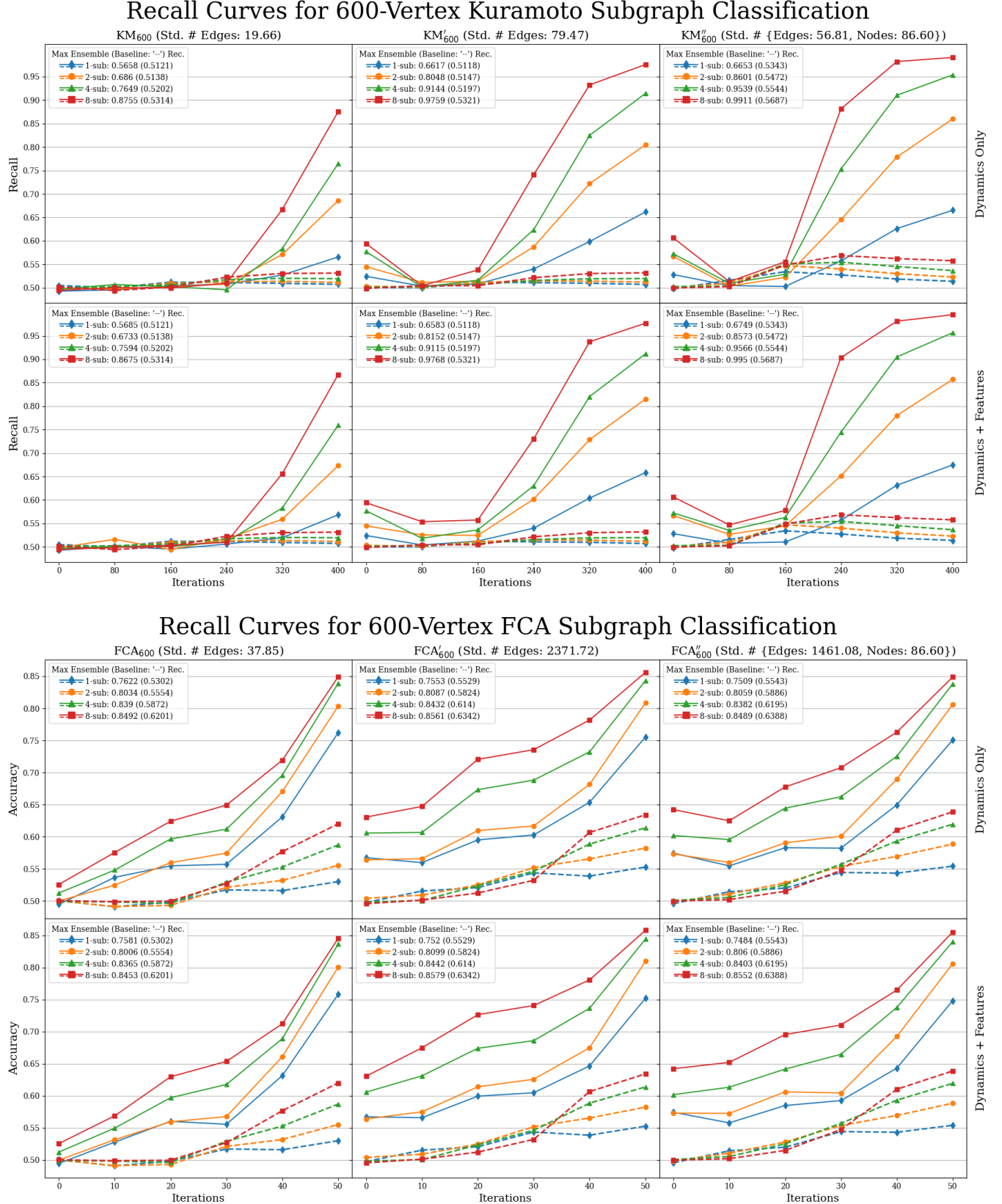
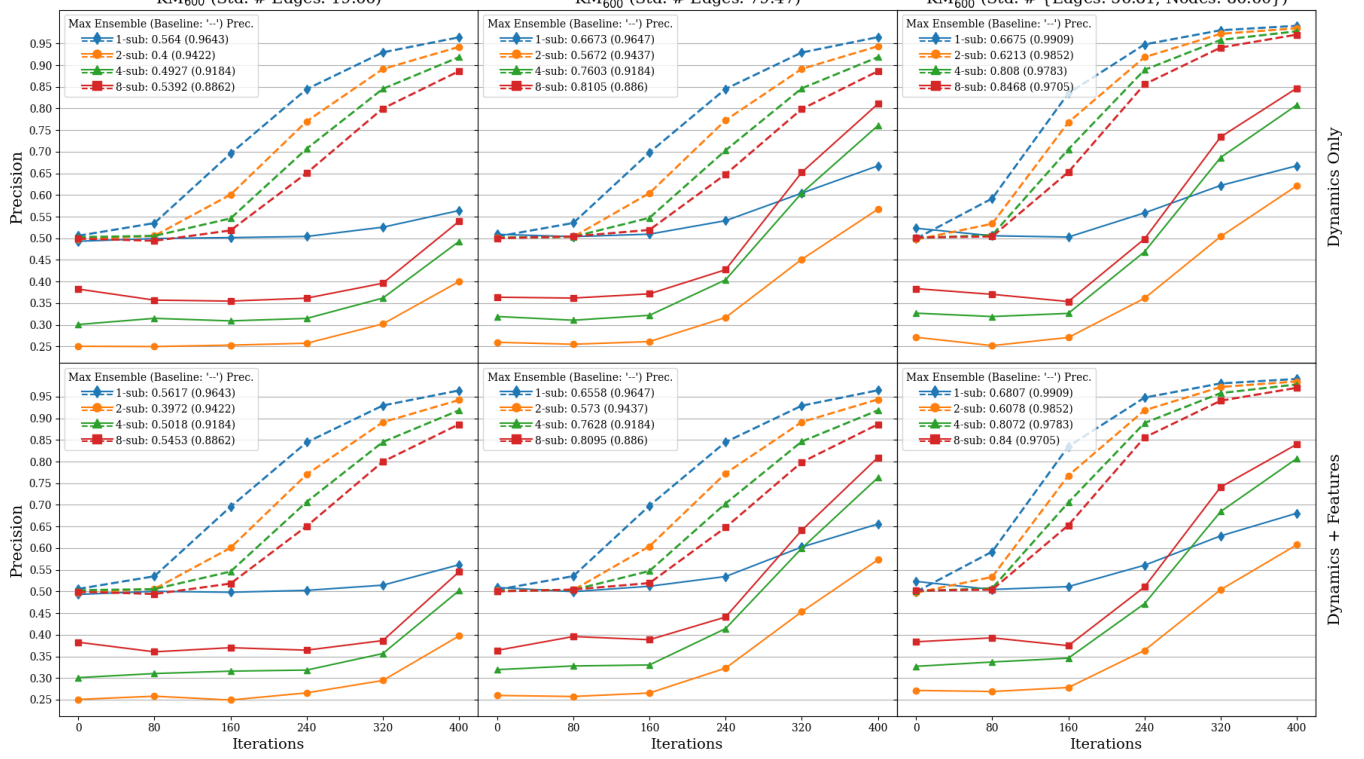


FIG. 11. Recall curves for predicting synchronization of both Kuramoto (top) and 5-color FCA (bottom) on 600-node graphs from dynamics observed from $k \in \{1, 2, 4, 8\}$ subgraphs of 30 nodes. All plots observe the performance of both the ensemble machine learning (solid) and baseline (dashed) recall scores over increasing training iterations $r \in \{0, 80, 240, 320, 400\}$. The first row shows results using only dynamics whereas the second row includes both the dynamics and graph features. In the legends, maximum recall scores for using k subgraphs over all r are given by ' k -sub: Acc. (Baseline Acc.)'

Precision Curves for 600-Vertex Kuramoto Subgraph Classification



Precision Curves for 600-Vertex FCA Subgraph Classification

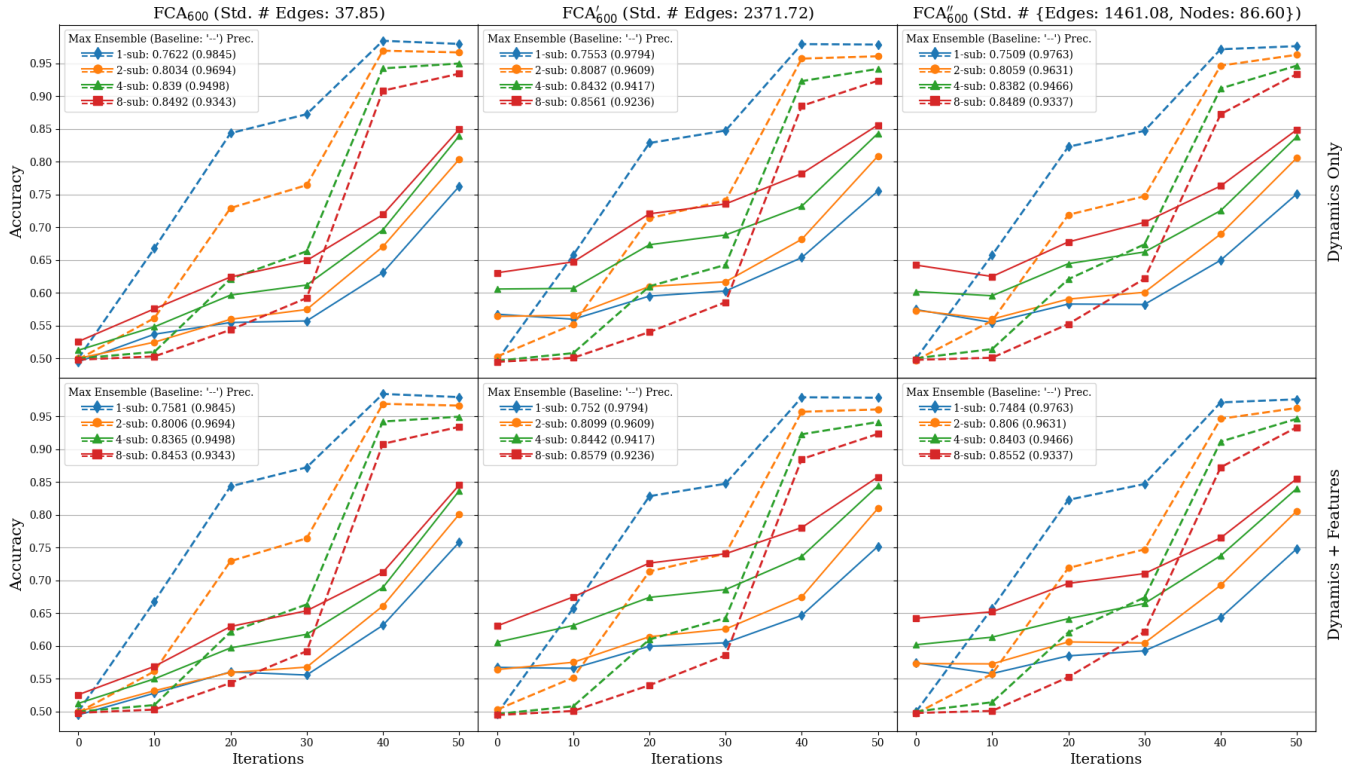


FIG. 12. Precision curves for predicting synchronization of both Kuramoto (top) and 5-color FCA (bottom) on 600-node graphs from dynamics observed from $k \in \{1, 2, 4, 8\}$ subgraphs of 30 nodes. All plots observe the performance of both the ensemble machine learning (solid) and baseline (dashed) precision scores over increasing training iterations $r \in \{0, 80, 240, 320, 400\}$. The first row shows results using only dynamics whereas the second row includes both the dynamics and graph features. In the legends, maximum precision scores for using k subgraphs over all r are given by 'k-sub: Acc. (Baseline Acc.)'